Journal of Colloid and Interface Science 455 (2015) 226–235

Contents lists available at ScienceDirect

Journal of Colloid and Interface Science

www.elsevier.com/locate/jcis

The retention of liquid by columnar nanostructured surfaces during quartz crystal microbalance measurements and the effects of adsorption thereon

Keith B. Rodenhausen [a,*], Ryan S. Davis [a], Derek Sekora [a], Dan Liang [a], Alyssa Mock [a], Rajeev Neupane [a], Daniel Schmidt [a,b], Tino Hofmann [a], Eva Schubert [a], Mathias Schubert [a]

[a] Department of Electrical and Computer Engineering and Center for Nanohybrid Functional Materials, University of Nebraska-Lincoln, Lincoln, NE 68508, USA
[b] Singapore Synchrotron Light Source, National University of Singapore, Singapore 117603, Singapore

GRAPHICAL ABSTRACT

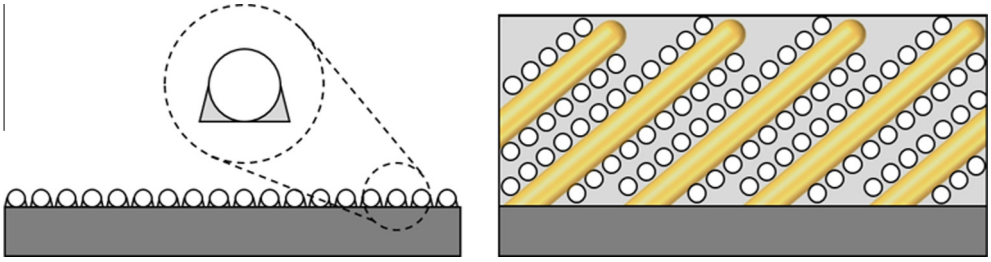

ARTICLE INFO

Article history:
Received 3 April 2015
Accepted 20 May 2015
Available online 3 June 2015

Keywords:
Quartz crystal microbalance
Generalized ellipsometry
Solid–liquid interface
Nanostructured surface
Adsorption
Porosity

ABSTRACT

Hypothesis: A surface comprising spatially coherent columnar nanostructures is expected to retain intercolumnar liquid during a quartz crystal microbalance measurement due to the surface structure. Part of the liquid retained by the nanostructures may then be displaced by adsorbate.

Experiments: Slanted columnar nanostructure thin films were designed to vary in height but remain structurally similar, fabricated by glancing angle deposition, and characterized by generalized ellipsometry. A frequency overtone analysis, introduced here, was applied to analyze quartz crystal microbalance data for the exchange of isotope liquids over the nanostructured surfaces and determine the areal inertial mass of structure-retained liquid. The adsorption of cetyltrimethylammonium bromide onto nanostructures was investigated by simultaneous quartz crystal microbalance and generalized ellipsometry measurements.

Findings: The areal inertial mass of structure-retained liquid varies linearly with nanostructure height. The proportionality constant is a function of the surface topography and agrees with the generalized ellipsometry-determined nanostructure film porosity, implying that nearly all intercolumnar liquid is retained. We report that for adsorption processes within porous nanostructured films, the quartz crystal microbalance is sensitive not to the combined areal inertial mass of adsorbate and retained liquid but rather to the density difference between adsorbate and liquid due to the volume exchange within the nanostructure film.

* Corresponding author.
E-mail address: kbrod@engr.unl.edu (K.B. Rodenhausen).

http://dx.doi.org/10.1016/j.jcis.2015.05.038
0021-9797/

1. Introduction

Adsorption and desorption processes [1–3], surface chemical reactions [4,5], and reorganization of chemical species [6,7] and the kinetics thereof are widely studied at the solid–liquid interface. Thus far, such processes are commonly studied on flat surfaces. The quartz crystal microbalance (QCM) technique is used to monitor these processes and allows for the determination of the areal inertial mass (i.e., surface inertial mass density) of an adsorbate layer. In addition to adsorbate, the layer may comprise liquid that hydrates, for example, and is retained by the adsorbate. It is well-known that QCM measurements do not permit the differentiation between the areal inertial mass of adsorbate and the retained liquid on flat surfaces, and it is often reported that QCM data analysis "overestimates" the areal inertial mass of adsorbate [1,6,8–10]. Optical techniques such as ellipsometry [7,8,11–13], reflectometry [14,15], surface plasmon resonance spectroscopy [16,17], and dual-polarization interferometry [18,19] have also been used to monitor adsorption of organic molecules independently of or in conjunction with QCM or a further development of QCM known as quartz crystal microbalance with dissipation (QCM-D). The use of an optical technique in tandem with QCM or QCM-D may allow for the determination of the adsorbate layer porosity [20–22].

Three-dimensional (3D) spatially coherent nanostructured films, such as slanted columnar thin films (SCTFs) produced by glancing angle deposition (GLAD) [23,24], are emerging as scaffolding materials upon which adsorption processes may be evaluated [25–28]. SCTFs have many advantages over flat surfaces; SCTFs have increased surface area, have spatial dimensions that may be controlled by their fabrication process [23,24,29], may act as molecular filters or storage [27,28], have strongly anisotropic optical properties for sensor applications [26,30,31], provide improved biocompatibility with cells due to their topography [25,28], and may be fabricated from materials that result in films exhibiting the surface-enhanced Raman scattering (SERS) effect [32].

It is hypothesized here that liquid within a SCTF may be retained in the absence of adsorbate by the oscillating nanostructures during a QCM measurement. Thus, adsorbate that attaches within a SCTF during a QCM measurement may not retain further liquid and may liberate displaced liquid that was formerly retained. The different mechanisms of liquid retention between flat and SCTF surfaces may provide an avenue for QCM to differentiate between adsorbate and retained liquid without the need for additional techniques.

Martin et al. used flat and rough surfaces to simultaneously determine the density and viscosity of liquids by QCM, alone [33]. The difference between flat and SCTF surfaces on the amount of liquid retained during a QCM measurement in the presence of adsorbate is illustrated by Fig. 1. The purpose of this work is to determine whether all, part, or none of the liquid within a SCTF is retained during QCM measurement. Additionally, it must be determined whether an adsorption process into a SCTF has an additive, neutral, or deleterious effect on the areal inertial mass of retained liquid.

QCM is a mechanical technique whereby a piezoelectric AT-cut quartz crystal sensor oscillates in a shear mode at its resonance frequency under an applied alternating potential. Variations of the areal inertial mass and variations of the bulk liquid density and viscosity modulate the frequency of oscillation ν. Existing approaches to model the effects of liquid properties on the QCM response become unsuitable as random surface roughness increases [34]. SCTFs, however, are "super-rough" surfaces and thus require the advancement of existing data analysis approaches, which may allow for the determination of areal inertial mass of retained liquid in highly ordered 3D nanostructure thin films.

The use of deuterated liquids to determine the porosity and areal inertial mass of an adsorbate layer on a flat surface with QCM, alone, was introduced by Craig and Plunkett [35]. This method requires the surface to be measured under a liquid and the liquid's deuterated analog before and after adsorbate layer formation. The deuterated liquid is assumed to be chemically identical to non-deuterated liquid and has a larger density. If the QCM chamber ambient is changed from air to liquid, the QCM-measured frequency shift is ideally larger for the deuterated liquid than the non-deuterated liquid. However, the processes of filling the QCM chamber with liquid or emptying liquid out of the chamber may cause irreproducible frequency shifts due to pressure changes. Instead, the deuterated and non-deuterated liquids may be cycled through the QCM chamber to more closely maintain isobaric conditions. One thus measures the two frequency shifts between (a) the bare surface exposed to deuterated and non-deuterated liquids and (b) the surface with adsorbate exposed to deuterated and non-deuterated liquids (alternatively a bare surface exposed to deuterated and non-deuterated liquids with dissolved adsorbate). These measurements allow for determination of the fraction of the frequency shift between the bare surface and the surface with adsorbate under non-deuterated liquid that is due to retained liquid rather than adsorbate [35]. This strategy has been used to quantify the areal inertial mass and porosity of organic layers, including polyelectrolyte multilayers [36] and polysaccharides [37–39]. Due to its highly ordered geometry and porous structure, a mechanically oscillating SCTF interacts with the bulk liquid differently than a flat surface, and so the method of Craig and Plunkett may not be readily applicable. Additional theoretical work is required for the analysis of QCM data for highly ordered 3D surfaces. Specifically, the capability to quantify retained liquid, which may be described by a porosity parameter intrinsic to the SCTF geometry, is desired.

Generalized ellipsometry (GE) is an optical technique that measures the change of the polarization state of light after it reflects off of or transmits through a sample, particularly anisotropic materials such as SCTFs [40,41]. GE measures elements of the 4×4 Mueller

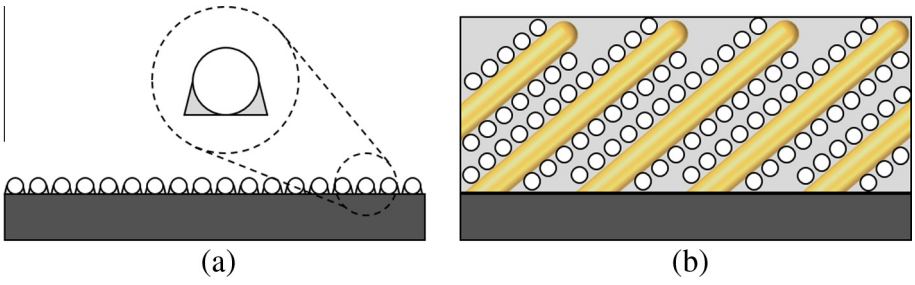

Fig. 1. (a) Adsorbate (here depicted by particles) attached to a flat surface. During QCM measurement, each particle retains liquid (shaded). In this case the retained liquid may be arranged, for example, in a conal distribution. Alone, QCM is generally not sensitive to the distribution of retained liquid or to the areal inertial mass ratio of adsorbate to retained liquid. (b) Adsorbate particles attached to a SCTF. During QCM measurement, liquid is retained by the nanostructured surface. Liquid retention by the SCTF implies that adsorbate displaces retained liquid and hence partially offsets the measured frequency shift.

matrix **M**, which completely describe the optical response of the experimental system. Samples are considered as plane-parallel layer stacks in an optical model. Physical properties of interest, including the height parameters and dielectric functions of constituent layers, are variables of the optical model. Mueller matrix element spectra are calculated for each optical model iteration until the calculated and measured Mueller matrix element spectra best match. The model parameters for the best-matching model-calculated spectra are thus considered to describe the sample. GE is very sensitive to the birefringence and dichroism of SCTFs and has been used to quantify SCTF structural properties, SCTF volume fraction compositions (i.e., porosity), and adsorption processes onto SCTFs [13,26,40–44]. GE is used here as a reference technique to characterize SCTF structural properties and the fraction parameters of liquid and adsorbate.

In this work, a frequency overtone analysis (FOA) is introduced to quantify the amount of liquid retained by SCTFs during QCM measurements. Four SCTF samples varying in height, i.e., columnar length, but otherwise structurally similar were fabricated by GLAD [23,24] and characterized by GE [40–43]. During QCM measurement, the SCTFs were cyclically exposed to H_2O and D_2O. The FOA, developed here and further discussed below, was applied to quantify the areal inertial mass of retained liquid associated with each oscillating SCTF from QCM data analysis. We find that the amount of retained liquid varies linearly with the SCTF height. The proportionality constant, termed here the "differential retained liquid areal inertial mass per differential columnar height" (γ), is an intrinsic parameter that may be used to characterize the topography or porosity of surfaces that consist of highly ordered 3D nanostructures. The retained liquid is interpreted to be coupled not to individual nanostructures but rather within the near-range network of nanostructures. The porosity parameter derived from our QCM isotope exchange technique (γ) is in excellent agreement with the best-match model porosity parameters obtained from GE data analysis for all samples investigated here. Additionally, the adsorption of cetyltrimethylammonium bromide (CTAB), a cationic surfactant, onto a SCTF was monitored by QCM and GE. It is found that GE reports at least three times as much adsorbate areal inertial mass as QCM. This finding demonstrates that QCM has different sensitivity to adsorbate depending on whether the substrate is flat or nanostructured.

2. Frequency overtone analysis

A frequency overtone analysis (FOA) is introduced here that enables the determination of an areal inertial mass parameter of liquid retained by surfaces consisting of highly ordered 3D nanostructures during QCM measurements.

Many QCM instruments are capable of measuring multiple overtones of order N, where $N = 3, 5, \ldots$, of the fundamental resonance frequency of the quartz sensor. QCM-D periodically turns off the driving potential of the sensor and monitors the signal decay with time. The decay is represented by the dissipation parameter D, which is indicative of changes in the damping properties of the experimental system [45–47]. Generally, decreases in ν and increases in D imply increases of adsorbate areal inertial mass and of dissipative (or viscous) losses of the system, respectively. Similarly to the observations reported by Rechendorff et al., the δD_N shifts here generally overlap after being multiplied by $\sqrt{N}$, and it will be shown that δD_N shifts are similar in magnitude for all investigated samples [34]. Hence, δD_N data are not considered for the FOA.

The Sauerbrey equation was developed previously for flat surfaces and describes the linear dependence of $|\delta\nu_N|$ on N [48]. Frequency shifts are interpreted to be caused by changes of a loaded inertial mass rigidly coupled to the oscillating surface. Because the average mean free path of water molecules at room temperature, which is considered here to be on the length scale of a hydrogen bond, does not exceed a few Angstroms [49], from the perspective of an individual molecule the nanostructure surfaces of a SCTF may be considered locally flat. Hence, the Sauerbrey equation is used here to consider liquid that is retained by SCTFs oscillating during QCM measurement.

The Sauerbrey equation is given by

$$\delta\Gamma = \frac{\delta m}{A} = -k\frac{\delta\nu_N}{N}, \tag{1}$$

where m is the rigidly coupled (loaded) mass, A is the surface area, and $\delta\Gamma$ is the change of rigidly coupled areal inertial mass. k is a constant defined as

$$k = \frac{\sqrt{\rho_q\mu_q}}{2\nu_0^2}, \tag{2}$$

where ν_0 is the fundamental frequency of the quartz sensor, ρ_q is the density of quartz, and μ_q is the shear modulus of quartz [48]. For an AT-cut quartz crystal with a fundamental frequency ν_0 of 5 MHz, k is generally considered to be 0.18 mg/(m^{2}Hz) [10]. $\delta\Gamma$ is linear with the overtone frequency, and all measured frequency shifts result in the same value when normalized by N [50,51].

The Borovikov equation (also known as the Kanazawa equation) was developed previously for flat surfaces and describes the square-root dependence of $|\delta\nu_N|$ on N [52,53]. Frequency shifts are interpreted to be caused by changes of viscosity and density of bulk liquid that resists the oscillating surface. The Borovikov equation is used here to consider bulk liquid effects due to liquid exchange over SCTFs oscillating during QCM measurement.

The Borovikov equation is given by

$$\delta\left(\sqrt{\rho_{liq}\eta_{liq}}\right) = -\frac{\sqrt{\pi\rho_q\mu_q}}{\nu_0^{3/2}}\frac{\delta\nu_N}{\sqrt{N}}, \tag{3}$$

where ρ_{liq} is the liquid density and η_{liq} is the liquid viscosity [52]. Here, the overtone frequency is linear with $\sqrt{\rho_{liq}\eta_{liq}}$ and proportional to the square root of the overtone order N [34,54].

For QCM liquid-phase experiments, one typically cannot determine the areal inertial mass of liquid retained by the surface because the QCM-measured frequency shift from air ambient to liquid ambient perturbs the pressure in the QCM chamber. The goal of this work is to determine this areal inertial mass, however, for highly ordered 3D surfaces. Exchange of liquids with different chemical properties and hence with different densities may result in different chemical interactions with the surface, which may affect the amount of liquid retained by the surface. The only accessible pathway for exchange of chemically equivalent liquids with different densities is the exchange of isotopes. Therefore we use an isotope-variation liquid-exchange approach in this work. That is, we cyclically expose SCTF surfaces to H_2O and D_2O. Hence we consider the frequency shifts during isotope exchange over a highly ordered 3D surface to be caused by a combination of Sauerbrey-like and Borovikov-like contributions, and we introduce and implement a FOA to separate and quantify these two effects.

For the case of a SCTF exposed to exchanged isotope liquids, we suggest that this combination of Sauerbrey-like and Borovikov-like contributions is sufficient to explain the QCM-measured $\delta\nu_N$ shifts, as will be shown below. Each contribution provides a share of $\delta\nu_N$ normalization by a different power of N (N and $\sqrt{N}$ for the Sauerbrey-like and Borovikov-like contributions, respectively).[1]

[1] Ideally, the higher overtone frequency shifts after such normalization are equivalent to measured $\delta\nu_1$. However, $\delta\nu_1$ is typically not measured or reported in the literature because the first overtone is most prone to experimental error, which is commonly related to the mechanical mounting of the quartz sensor [55,56].

Let a measured frequency shift $\delta\nu_N$ be described by the sum of Sauerbrey-like and Borovikov-like contributions $\delta\nu_{N,S}$ and $\delta\nu_{N,B}$, respectively,

$$\delta\nu_N = \delta\nu_{N,S} + \delta\nu_{N,B}. \tag{4}$$

Because $\delta\nu_{N,S}$ ($\delta\nu_{N,B}$) are proportional to N $\left(\sqrt{N}\right)$, Eq. (4) may be rewritten as

$$\delta\nu_N = \delta\nu_{1,S}N + \delta\nu_{1,B}\sqrt{N}. \tag{5}$$

The Sauerbrey-like and Borovikov-like contributions for the first harmonic overtone may be redefined as

$$\delta\nu_{1,S} = C\delta\nu_1, \tag{6}$$

$$\delta\nu_{1,B} = (1-C)\delta\nu_1, \tag{7}$$

respectively. C is a constant yet to be determined that has the same value for all harmonic overtones and distributes the relative weight given to the Sauerbrey-like and Borovikov-like contributions. Eq. (5) may be rewritten to yield

$$\delta\nu_1 = \frac{\delta\nu_N}{CN + (1-C)\sqrt{N}}. \tag{8}$$

Experimentally, one may find the value of C by varying its value between zero and unity until the right-hand side of Eq. (8) overlaps best with $\delta\nu_1$ for all measured overtones. Note that parameters C and $\delta\nu_1$ are overdetermined if more than two overtones are measured.

The experimentally determined change in the retained liquid areal inertial mass variation from isotope exchange $\delta\Gamma_\Delta$, where the superscript denotes the identity of the liquid, is written in the form of Eq. (1),

$$\delta\Gamma_\Delta \equiv \delta\Gamma^{D_2O} - \delta\Gamma^{H_2O} = -kC\delta\nu_1. \tag{9}$$

Let the ratio of the areal inertial mass variations be introduced as

$$y \equiv \frac{\delta\Gamma^{D_2O}}{\delta\Gamma^{H_2O}}. \tag{10}$$

It is necessarily assumed that the volume occupied by the retained liquid stays constant during isotope exchange, which implies that y is equal to the ratio of densities ρ^{D_2O}/ρ^{H_2O}, which can be obtained from the literature. At 20 °C, ρ^{H_2O} and ρ^{D_2O} are 0.9982 g/mL and 1.1053 g/mL, respectively [57]. Here $y = 1.1073$. Substitution of Eq. (10) into Eq. (9) yields

$$\delta\Gamma^{H_2O} = \frac{\delta\Gamma_\Delta}{y-1}. \tag{11}$$

For the case of a SCTF, one may consider $\delta\Gamma_{SCTF}$, the mass variation of retained liquid normalized by the SCTF surface area, or $\delta\Gamma$, the mass variation of retained liquid normalized by the (flat) substrate surface area. $\delta\Gamma_{SCTF}$ is found by considering the ratio of the flat reference substrate surface area A under the SCTF to the rough surface area A_{SCTF}, such that

$$\delta\Gamma_{SCTF} = \delta\Gamma\frac{A}{A_{SCTF}} = -kC\frac{\delta\nu_N}{N}\frac{A}{A_{SCTF}}. \tag{12}$$

The quantity of liquid confined within open volumes of SCTFs with cross-sections that are homogeneous across the film regardless of SCTF height is expected to be linear with respect to the SCTF height. Therefore we can define a parameter γ as the differential retained liquid areal inertial mass variation per differential columnar height,

$$\gamma \equiv \frac{\partial}{\partial d}\left(\delta\Gamma^{H_2O}(d)\right) \cong \frac{\Delta\delta\Gamma^{H_2O}}{\Delta d}. \tag{13}$$

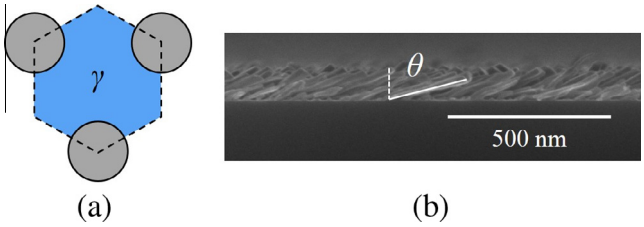

Fig. 2. (a) Top-down view schematic of a SCTF cross-section where liquid is retained by a near-range network of three nanocolumns (shaded circles). This schematic considers the scenario where all the liquid within the SCTF is retained. γ is shown in this example as the area of the liquid region multiplied by the liquid density divided by the area of the hexagonal unit cell. Note that the nanostructures do not have to be ordered, for example in a hexagonal arrangement, for γ to be determined. (b) Scanning electron microscopy image of a representative Ti SCTF. The angle between the nanostructures and the substrate normal is θ, and it is shown in this work that $\delta\Gamma^{H_2O}$ does not depend on θ.

As one possible interpretation of γ, we consider that liquid is not retained by individual nanostructures but by the near-range network of nanostructures that are not necessarily ordered. This interpretation is illustrated as a schematic by Fig. 2.

In this work, the nanostructures are considered as surface roughness. However, roughness on different scales can be additionally considered. Daikhin et al. defined "strong" and "slight" types of roughness, where for strong roughness the length scale of the roughness deviating from the reference plane is larger than the length scale in the lateral dimension; the opposite holds for slight roughness [58]. Here, the columnar nanostructures could be considered as strong roughness while the roughness of an individual nanostructure could be considered slight roughness. We assume here that roughness-derived effects on the measured QCM frequency shift are dominated by the strong roughness of the nanostructure layer. The roughness of an individual nanostructure is therefore neglected, here, but could be considered by future work.

It is now of interest to determine whether γ is constant with respect to d (i.e., there is a linear relationship between $\delta\Gamma^{H_2O}$ and d) or not and whether γ addresses the entirety of liquid within the SCTF or if a portion of liquid within the SCTF is not retained. For these purposes, we study the effect of isotope-variation liquid exchange over SCTFs of similar geometry, that is of similar cross-sectional area, but of different height. We also determine the void fraction (porosity) of the SCTFs by an optical method (GE). GE has been previously used to quantify protein adsorption onto SCTFs [26], characterize SCTF structural and optical properties after polymer infiltration [31], and monitor the swelling and deswelling of polymeric brushes anchored onto SCTFs [27,59].

3. Materials and methods

3.1. Isotope liquid exchange

The objective of the following experiments is to apply the FOA to determine $\delta\Gamma^{H_2O}$ and γ for a "family" of SCTFs designed to vary only by SCTF height d. We fabricated the SCTFs by electron-beam GLAD, a bottom-up fabrication technique that employs a physical vapor deposition process whereby the trajectory of an evaporated particle flux forms an oblique angle with the sample substrate normal. GLAD allows the formation of highly ordered films comprising nanostructures that are structurally highly equivalent except for length while sharing similar shape, diameter, and slanting angle. Discrete nanostructures are formed by geometrical shadowing, whereby initial nucleation sites block the areas behind them from the particle flux, and adatomic diffusion processes [23]. The Ti

SCTFs were deposited on commercially available Au-coated QCM sensors (Biolin Scientific).

An M-2000-VI spectroscopic ellipsometer (J.A. Woollam Co.) with a spectral range of 400–1640 nm was used to characterize the SCTFs. GE measurements were conducted at 45°, 55°, 65°, and 75° angles of incidence with respect to the substrate normal. For each angle of incidence, the sample was rotated from 0° to 360° in 6° increments, and a GE measurement was taken at each increment. A stratified optical model comprising an isotropic Au substrate, an anisotropic SCTF, and void ambient was used to calculate Mueller matrix element spectra. For example, the optical response of the SCTF is modeled here by an anisotropic Bruggeman effective medium approximation (ABEMA); the ABEMA describes physical properties of the SCTF including the SCTF height and constituent volume fractions (e.g., Ti and ambient) [44].

Varied parameters of the optical model were the ABEMA layer height d_{GE}, the void fraction of the ABEMA layer $f_{GE,void}$, the nanostructure slanting angle θ_{GE}, the ABEMA depolarization factors L_j (where $j = x, y, z$), the ABEMA monoclinic angle β, and the Ti dielectric function [60].

18.2 MΩ cm nanopure water (Barnstead Nanopure) and 99.9% D_2O (Sigma–Aldrich) were the liquids used for the isotope liquid exchange study. The liquid cell flow modules for E1 and E4 QCM-D instruments (Biolin Scientific) allow temperature control, and all measurements were taken at 20 °C. Fluid was pumped through the liquid cells at a rate of 0.1 mL/min. E1 QCM-D measurements on a flat sample began as H_2O was pumped through the liquid cell. Three cycles of D_2O and H_2O exchanges followed. Stable frequency signals were achieved before the next liquid exchange. This experiment was repeated with an E4 QCM-D for four SCTFs of different heights. Following QCM-D measurements, SCTF samples were characterized by scanning electron microscopy (SEM).

3.2. Surfactant adsorption

It is hypothesized here that Eq. (1) will underestimate the areal inertial mass of adsorbed CTAB because Eq. (1) does not consider liquid retained by surface structure prior to the adsorption process. The adsorption of CTAB is expected to liberate retained liquid and thereby partially offset the $\delta\nu_N$ shift reported by QCM. GE has been used to quantify the areal mass of organic adsorbates and is used here as a reference technique [26].

A Ti SCTF was fabricated by GLAD, characterized by GE, and optically modeled as described above. Four additional GE measurements were taken by an M-2000-V spectroscopic ellipsometer (J.A. Woollam Co.) with a spectral range of 400–1000 nm. GE measurement "A" was taken of the SCTF at a single sample orientation; that is, the sample was measured at one rotation angle and at a single (65°) angle of incidence. The Ti SCTF was then placed in a similar orientation within a windowed QCM liquid flow module with a 65° angle of incidence, which allows for simultaneous ellipsometry measurements, and GE measurement "B" was taken in the absence of liquid. H_2O was pumped into the flow module, and then GE measurement "C" was taken. At this point, QCM measurement began. Once stable QCM signals were achieved, an aqueous solution of 2.5 mM CTAB (Sigma–Aldrich) was pumped through the liquid cell. Once the QCM signal restabilized, GE measurement "D" was taken.

A stratified optical model comprising an isotropic Au substrate, a three-component (Ti, adsorbate, and ambient) ABEMA layer, an adsorbate layer, and ambient was used to calculate Mueller matrix element spectra. The model thus considers adsorbate that forms a layer on top of the SCTF in addition to adsorbate that infiltrates the SCTF. Optical model parameter values for the multiple-orientation GE measurement were used as starting points for the optical model parameters for GE Measurement A. For GE Measurement B, window offset parameters were introduced and varied in the optical model. For GE Measurement C, the ambient material was changed from void to water, and d_{GE}, f_{GE,H_2O}, θ, L_j, β, and the Ti dielectric function were varied in the optical model. To ensure the model is sensitive to the addition of adsorbate, the adsorbate volume fraction parameter f_{ads} was subsequently allowed to vary; the model thus yielded a f_{ads} value of 0.5% in the absence of adsorbate. Finally, for GE Measurement D, f_{ads} and the adsorbate layer height d_{ads} were varied from starting points of zero to account for the addition of adsorbate. The inertial areal mass of adsorbate over the flat substrate is given by the equation

$$\Gamma_{GE} = \rho_{ads} f_{ads} d_{GE}, \tag{14}$$

where ρ_{ads} is the density of adsorbate [26]. To estimate the values of ρ_{ads} and the adsorbate index of refraction n_{ads}, which are not readily available for CTAB, we used values for the similar molecule 2,2-dimethyloctadecane. Here values of 0.78 mg/mL for ρ_{ads} and 1.43 for n_{ads} are used [61].

4. Results

4.1. Isotope liquid exchange

For the isotope exchange experiments, Fig. 3 shows representative raw QCM-D results. The replacement of H_2O with denser D_2O causes $\delta\nu_N$ to decrease and δD_N to increase. Fig. 3 shows that the measurement signals stabilized more quickly when H_2O replaced D_2O than for the reverse process.

$\delta\nu_N$ measured experimentally for the flat surface are shown in Fig. 4 and overlap with a C value very close to 0, indicating that the frequency shift is caused by bulk liquid effects rather than liquid retention ($\delta\nu_1 = -118$ Hz, $C = 0.014$). The δD_N shifts for the flat and SCTF surfaces are similar in magnitude, and we do not consider δD_N data further.

Fig. 5 displays results for the SCTF samples. $\delta\nu_1$ and C are determined simultaneously by the FOA; the $C = 0$ and $C = 1$ lines in Fig. 5 show the calculated overtone dependence of $\delta\nu_N$ for the Borovikov and Sauerbrey cases, respectively. $\delta\nu_N$ for the SCTFs overlap after normalization by both N and $\sqrt{N}$ components. The highest overtones ($N = 11,\ 13$) generally do not follow the trends of the other overtones and were omitted from the FOA. It has been reported that the higher overtones are less reproducible than $N = 3$ [62,63]. C, $\delta\nu_1$, and $\delta\Gamma^{H_2O}$ vary with respect to columnar height, and C values are shown with Fig. 5. C and $\delta\nu_1$ increase with respect to columnar height, but not linearly.

Fig. 6 shows $\delta\Gamma^{H_2O}$ as a function of d_{GE}, and a linear relationship is found such that

$$\delta\Gamma^{H_2O} = (0.740 \pm 0.039)\frac{\text{mg}}{\text{m}^2\ \text{nm}} d_{GE}. \tag{15}$$

SCTF height determined by SEM and SCTF structural parameters parameters from optical modeling are shown in Table 1. It is found from the GE analysis that the porosity $f_{GE,void}$ stays fairly constant while the slanting angle θ changes. Fig. 7 shows cross-sectional SEM images of the SCTF samples for the determination of the height d_{SEM}.

4.2. Surfactant adsorption

For the CTAB adsorption measurements, raw QCM $\delta\nu_N$ data are shown by Fig. 8. Fig. 8 shows that the frequency overtones do not perfectly overlap. Thus, determining the mechanical adsorbate areal inertial mass $\Gamma_{GE,QCM}$ with Eq. (1) depends on which overtone

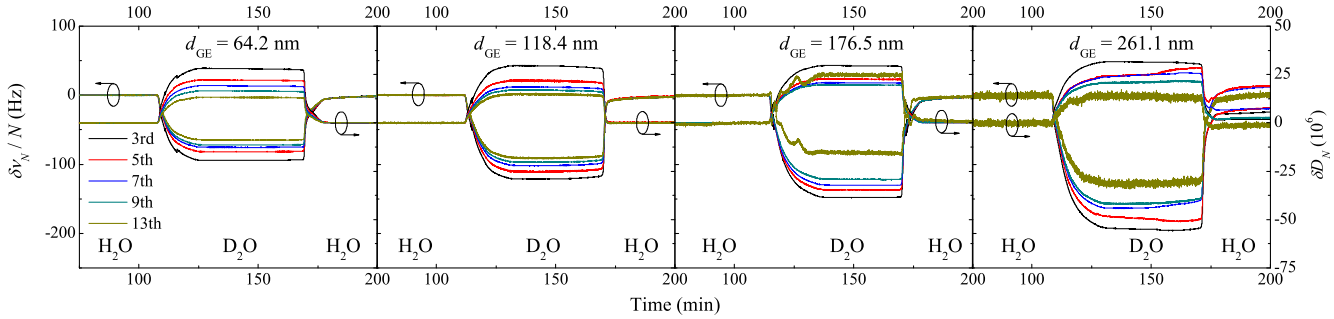

Fig. 3. $\delta\nu_N/N$ (left axis) and δD_N (right axis) during sample exchange of H_2O and D_2O over SCTFs. H_2O and D_2O enter the liquid cell during regimes labeled "H_2O" and "D_2O," respectively. A d_{GE} value from Table 1 is shown for each sample.

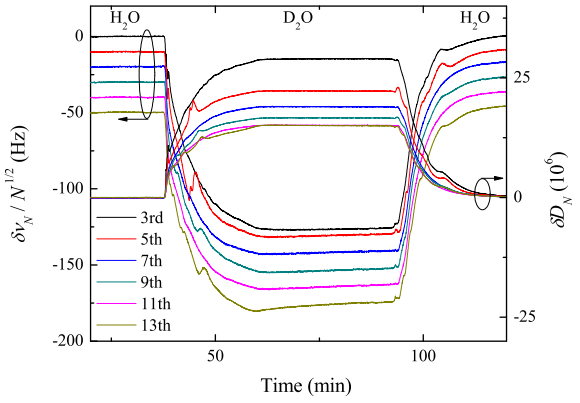

Fig. 4. $\delta\nu_N/\sqrt{N}$ (left axis) and δD_N (right axis) during sample exchange of H_2O and D_2O over a flat Au surface. H_2O and D_2O enter the liquid cell during regimes labeled "H_2O" and "D_2O," respectively. $\delta\nu_N$ shifts for each successive overtone are offset by 10 Hz for clarity.

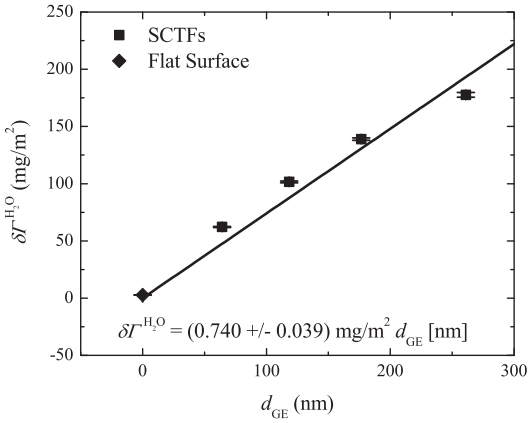

Fig. 6. $\delta\Gamma^{H_2O}$ as a function of d_{GE}. The result for the flat surface is included for the linear regression.

is selected. $\Gamma_{QCM,ads}$ was obtained for each measured overtone, and the average value of $\Gamma_{QCM,ads}$ is 2.6 mg/m^2.

SCTF structural parameters from the GE optical modeling are given in Table 2. Upon the addition of H_2O into the liquid cell (GE Measurement C, Table 2), the values of d_{GE}, the fraction parameters, and slanting angle θ shift. It is possible that capillary forces deformed the SCTF. The CTAB fraction parameter for GE Measurement D is 10.7%. Eq. (14) yields an optical adsorbate areal mass $\Gamma_{GE,ads}$ of 8.7 mg/m^2. The height of the adsorbate layer over the SCTF d_{ads} remained at zero for GE Measurement D. Thus the optical model considered all adsorbate to be within the ABEMA layer.

Fig. 9 shows Mueller matrix element spectra taken before (GE Measurement C) and after (GE Measurement D) CTAB adsorption. The spectra show sensitivity to the presence of CTAB.

5. Discussion

The major findings of this work are summarized here. First, a single γ value describes all four SCTF samples used for isotope liquid exchange. Second, nearly all the liquid within a SCTF is retained during QCM measurement. Third, the Borovikov-like contributions to the measured frequency shifts for the SCTF samples during isotope liquid exchange show good agreement with the measured frequency shift for the flat surface, where the flat surface reveals only Borovikov-like contributions. Fourth, adsorbate displaces retained liquid within SCTFs. Finally, the GE optical model reports that over three times as much adsorbate attaches to the nanostructures than that determined by traditional QCM data analysis approaches. One must consider that QCM detects changes in the areal inertial mass caused by the density difference between liquid retained by the oscillating SCTF and the incoming adsorbate that displaces it.

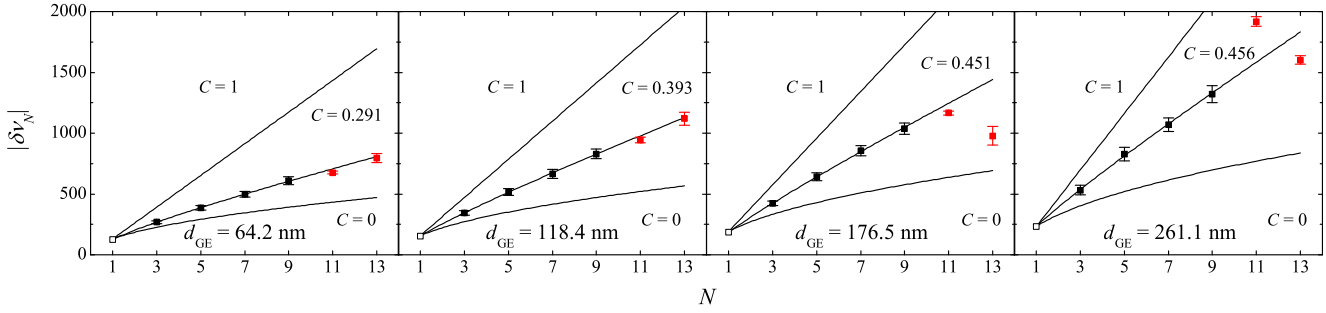

Fig. 5. $|\delta\nu_N|$ as a function of N. Filled symbols are experimental data, and open symbols are $|\delta\nu_1|$ determined by the FOA. Black filled symbols are considered for the FOA, and light (red for the online version of this contribution) filled symbols are omitted. The lines that emanate from the open $|\delta\nu_1|$ symbols predict the overtone dependance of $|\delta\nu_N|$ for a given C value. d_{GE} is shown for each sample. (For interpretation of the references to color in this figure legend, the reader is referred to the web version of this article.)

Table 1
Height parameters d_{SEM} and d_{GE}, void fraction parameters $f_{GE,void}$, Ti fraction parameters $f_{GE,Ti}$, and nanostructure slanting angles with respect to the substrate normal θ for all SCTF samples. d_{SEM} are obtained from SEM, and all other parameters are obtained from GE.

Parameter	FOA Sample 1	FOA Sample 2	FOA Sample 3	FOA Sample 4
d_{SEM} (nm)	73 ± 10	138 ± 17	197 ± 29	260 ± 35
d_{GE} (nm)	64.2 ± 0.1	118.4 ± 0.2	176.5 ± 0.3	261.1 ± 0.7
$f_{GE,void}$ (%)	79.7 ± 0.1	80.2 ± 0.1	78.8 ± 0.1	78.8 ± 0.1
$f_{GE,Ti}$ (%)	20.3 ± 0.1	19.8 ± 0.1	21.2 ± 0.1	21.2 ± 0.1
θ_{GE} (°)	66.8 ± 0.1	58.0 ± 0.1	55.2 ± 0.1	54.3 ± 0.1

5.1. SCTF retention of liquid during QCM measurement

The data plotted in Fig. 6, obtained from Figs. 3 and 5, suggest that there is a linear relationship between $\delta\Gamma^{H_2O}$ and d_{GE}. Due to this linearity, it is suggested here that γ, defined as the derivative in Eq. (13), is constant for all investigated samples and is equivalent to the slope of the line in Fig. 6. The units of γ refer to mass per unit area A per unit length of height d. Thus, the SCTF family has a γ value of 0.740 ± 0.039 mg/(m^2 nm). For Fig. 6, one could alternatively consider a line with a positive y-intercept and that does not consider the flat surface data point. We would interpret such behavior to be caused by SCTF structure non-idealities, specifically, the SCTF nucleation layer. At the beginning of the GLAD process, a seeding layer of small nucleation sites forms. As these nucleation sites enlarge, a competitive growth phase occurs, and fewer, larger structures emerge [23,24,29]. The deposited material shadowed by the larger structures, i.e., the nucleation layer, can be seen in the SEM images of Fig. 7. Future work could more closely investigate the dependence of $\delta\Gamma^{H_2O}$ on d, particularly for shorter SCTFs, to elucidate the effect of the nucleation layer on liquid retention.

γ is constant because the porosity of the nanostructures is constant with respect to nanostructure height, which is in agreement with the GE modeling results. That is, if one selects an infinitesimal cross-sectional sheet of a SCTF, as depicted in Fig. 2(a), the total nanostructure area is the same regardless of the position (height) of the sheet within the SCTF. Because θ_{GE} is not constant for all samples, the slanting angle does not affect the total nanostructure area of the infinitesimal cross-sectional sheet. γ is thus a measure of the area of the infinitesimal sheet that comprises retained liquid. Different nanostructure packing arrangements may affect the cross-sectional nanostructure area and thereby γ. $\delta\Gamma^{H_2O}$ does depend on d and by extension θ_{GE}. d may be considered a scaling factor for γ to yield $\delta\Gamma^{H_2O}$, as our earlier interpretation of γ in Eq. (13) implies.

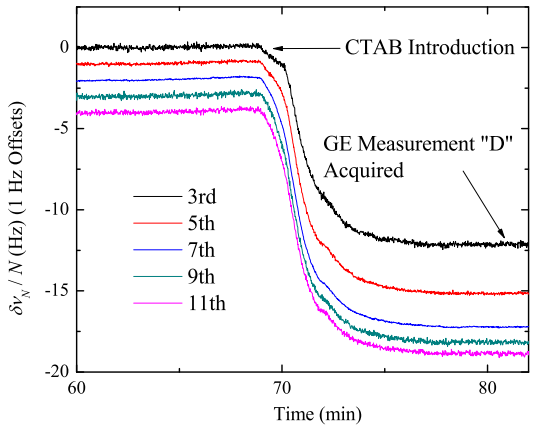

Fig. 8. QCM $\delta\nu_N$ data, normalized by N, for 2.5 mM CTAB adsorption onto Ti SCTF. Each successive overtone is offset by 1 Hz for clarity.

Table 2
Height parameters d_{GE}, H_2O fraction parameters f_{GE,H_2O}, Ti fraction parameters $f_{GE,Ti}$, CTAB fraction parameters $f_{GE,ads}$, and nanostructure slanting angles with respect to the substrate normal θ for GE Measurements C and D. All parameters are obtained from GE.

Parameter	GE Meas. C	GE Meas. D
d_{GE} (nm)	104.5 ± 0.1	104.5 ± 0.1
$f_{GE,H2O}$ (%)	85.2 ± 0.2	75.0 ± 0.2
$f_{GE,Ti}$ (%)	14.3 ± 0.1	14.3 ± 0.1
$f_{GE,ads}$ (%)	0.5 ± 0.2	10.7 ± 0.2
θ_{GE} (°)	51.5 ± 0.2	51.5 ± 0.2

The retained liquid should reside between rather than above the individual nanostructures because $\delta\Gamma^{H_2O}$ scales linearly with d_{GE} as shown in Fig. 6. Two alternate possibilities are that all or only part of the liquid within the SCTF is retained; these scenarios are referred to here as complete filling and partial filling, respectively. The fraction of total material composing the SCTF that is retained liquid is provided by γ. γ has units of mg/(m^2 nm), which converts to 1 g/mL. The scenario of complete filling implies the porosity is equal to γ/ρ^{H_2O}, and the scenario of partial filling implies the porosity is at least γ/ρ^{H_2O}.

To determine whether complete filling or partial filling is observed, we consider the GE modeling results. The average

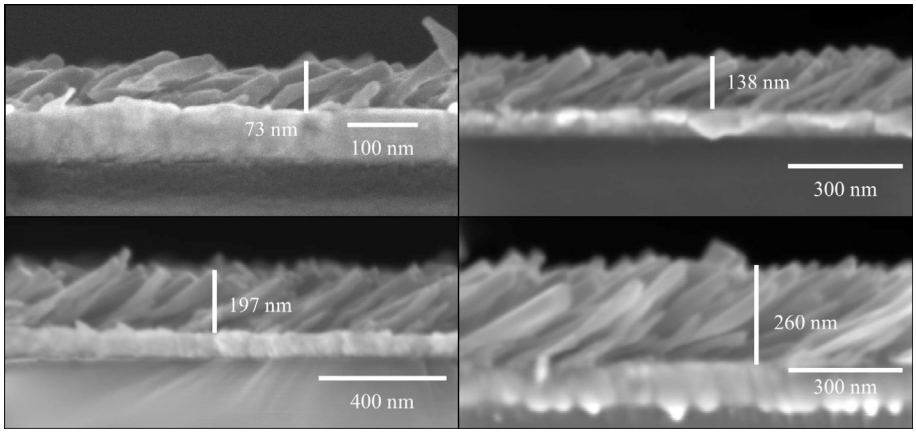

Fig. 7. Cross-sectional SEM images and d_{SEM} of SCTF samples.

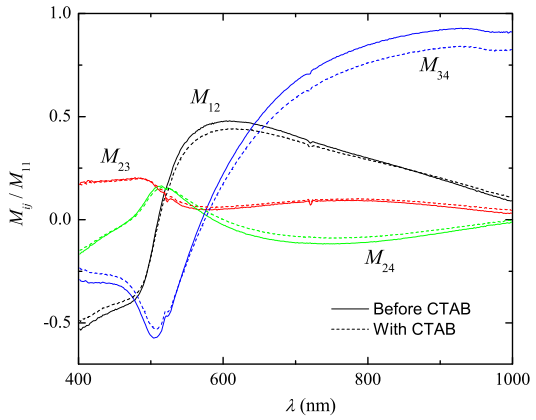

Fig. 9. Select Mueller matrix element spectra for before (GE Measurement C) and after (GE Measurement D) CTAB adsorption.

GE-derived porosity for the SCTFs is 79.6%, which is close to our observed γ (retained liquid fraction) value of 74.0%. It is therefore suggested here that a scenario of nearly complete filling holds.

SCTFs differing only by height will have different C values; their Borovikov-like contributions may be equivalent, but a SCTF with longer nanostructures will have a larger Sauerbrey-like contribution and thus a larger C value. $\delta\nu_1$ of a rough surface will be larger than $\delta\nu_1$ of a flat surface because although the oscillation of both surfaces is resisted by the bulk liquid, the rough surface is loaded with more retained liquid than the flat surface. Thus, C and $\delta\nu_1$ are not intrinsic parameters for SCTFs. $\delta\Gamma_{\mathrm{SCTF}}^{\mathrm{H_2O}}$ and γ are distinct in that γ is a function of the substrate surface coverage by nanostructures while $\delta\Gamma_{\mathrm{SCTF}}^{\mathrm{H_2O}}$ is not. As noted earlier, $\delta\Gamma^{\mathrm{H_2O}}$ scales with d. γ may therefore be used to classify the topography of a given highly ordered 3D nanostructured surface.

$\delta\Gamma^{\mathrm{H_2O}}$ may be determined by QCM experiments, alone, but determination of γ requires knowledge of the SCTF height. Depending on the sample, atomic force microscopy (AFM), SEM, or GE, for example, may be applied for this purpose. GE is particularly well-suited to characterize anisotropic SCTFs, such as those considered here [40–43].

It has been shown that the obtained Sauerbrey-like contributions to $\delta\nu_1$ can be evaluated by how well they describe the porosity of a SCTF. The Borovikov-like contributions to $\delta\nu_1$ for SCTFs may be evaluated by comparing them to $\delta\nu_1$ of the flat surface. The percent difference between $\delta\left(\rho_{\mathrm{liq}}\eta_{\mathrm{liq}}\right)^{1/2}$ evaluated for the flat surface from QCM data and predicted by Eq. (3) is found to be 2.8%. For the SCTFs, the average value of $(1-C)\delta\nu_1$, the Borovikov-like contribution to $\delta\nu_1$, is -103 ± 14 Hz, which has a 13.6% difference from $\delta\nu_1$ of the flat surface (-118 Hz). This difference is close and demonstrates that the FOA partitions the measured QCM frequency response between inertial mass loading and bulk liquid contributions by considering them as Sauerbrey-like and Borovikov-like effects, respectively. The Borovikov-like contributions to $\delta\nu_1$ of SCTF surfaces may be smaller in magnitude than $\delta\nu_1$ of the flat surface because there is less solid material at the SCTF-bulk liquid interface, and therefore the bulk liquid may resist SCTF oscillation less than for a flat surface.

The overall approach of the FOA is modular such that new modeling equations specific to 3D surface geometries may be implemented in the place of the Sauerbrey or Borovikov equations. For a modeling equation that considers fluid flowing around columnar structures rather than over a flat surface, as the Borovikov equation does, the frequency data might be normalized by a power of N other than 1/2 and thereby affect C. However, with our approach of matching $\delta\nu_N$ by sums of N in powers of 1 and 1/2, only, a nearly perfect match is obtained in Fig. 5 for the smaller overtones. Future work may vary SCTF spacing, for example, via surface pre-patterning [64,65] or pre-roughening methods [28], to determine if there is a limit for nanostructure proximity to retain all liquid within the SCTF. Other nanostructure geometries, such as chevrons, staircases, helices, screws, and vertical posts, could also be evaluated.

SEM and GE show some disagreement regarding the heights of the SCTFs. Because the nanostructures were grown on soft gold and also not along the crystalline axis of quartz sensor, the cleaving of the samples introduced uncertainty to the SEM height observations due to the breaking up of adjacent nanocolumns and subsequently apparent disorder in the SEM side view. Thus, and because the probe beam of the GE instrument (approximately 100 μm × 300 μm) samples over much larger sample areas, delivering more representative height parameters, the GE-determined height d_{GE} rather than d_{SEM} is considered throughout this work.

5.2. QCM sensitivity to adsorption on SCTFs

$\Gamma_{\mathrm{GE,ads}}$ (8.7 mg/m^2) is over three times as large as $\Gamma_{\mathrm{QCM,ads}}$ (2.6 mg/m^2). It is often reported in the literature that for organic adsorption processes onto flat surfaces, ellipsometry reports a smaller adsorbate layer $\delta\Gamma$ than QCM because ellipsometry is less sensitive to retained liquid (and not at all for ultra-thin layers on the scale of 10 nm or less in height) [6,11,20]. GE providing a larger adsorbate areal mass than QCM implies that QCM detects adsorbate differently on SCTF surfaces than flat surfaces.

Because nearly all the liquid within a SCTF is retained during a QCM measurement, adsorbate that attaches within the SCTF necessarily displaces liquid. If the excess volume V^E of mixed dissolved adsorbate and liquid is considered negligible for dilute solutions [66,67], then the volume of attached adsorbate is equivalent to the volume of displaced liquid. Thus, for adsorption processes into SCTFs, one expects that the QCM is not sensitive to the combined areal inertial mass of adsorbate and liquid retained by the adsorbate, as is the case for adsorption processes onto flat surfaces. Instead, QCM is sensitive to the change of density $\delta\rho$ of inertial mass within a volume where liquid and adsorbate are exchanged, as shown by

$$l_{\mathrm{ads}}\delta\rho\frac{A_{\mathrm{SCTF}}}{A} = l_{\mathrm{ads}}\left(\rho_{\mathrm{ads}}-\rho_{\mathrm{liq}}\right)\frac{A_{\mathrm{SCTF}}}{A} = -k\frac{\delta\nu_N}{N}, \tag{16}$$

where l_{ads} is the adsorbate contribution to the height of a mixed adsorbate/retained-liquid layer over a nanostructure surface, ρ_{ads} is the density of adsorbate, and ρ_{liq} is the density of liquid. The liquid contribution is ignored in Eq. (16) because all the liquid within the SCTF is already retained.

The density of CTAB is less than that of H_2O.[2] Thus, Eq. (16) implies that CTAB adsorption yields a positive frequency change, which is not reported by Fig. 8. CTAB adsorption onto the tips of the nanostructures may be the cause for this discrepancy. Fig. 7 shows that the nanostructure tips are not uniformly distributed. The best-match optical model for GE Measurement D considers all the CTAB within the ABEMA layer rather than on top. Because CTAB is a small molecule, about 2 nm long, and because the nanostructures are not uniform in height, it is reasonable that CTAB on the nanostructure tips would be considered within the ABEMA layer of the optical model. Liquid nearby the tips may not be retained by the oscillating SCTF because the nanostructures are not as spatially coherent at the tips. Therefore, CTAB adsorbing onto the tips and the liquid hydrating the CTAB could be sensed by QCM as a

[2] Sigma–Aldrich provides a density of 0.968 g/mL for 25 wt.% cetyltrimethylammonium chloride in H_2O at 25 °C.

Sauerbrey-like load. CTAB may not uniformly coat the SCTF. Preferential CTAB adsorption onto the SCTF tips would favor replacement of non-retained rather than retained liquid and hence a negative frequency shift. Additionally, the loss of spatial coherence at the tips may contribute to the difference between $f_{GE,void}$ and the porosity derived from γ.

The exchange of CTAB and nanostructure-retained liquid and the adsorption of CTAB onto the nanostructure tips constitute two simultaneous processes with opposing frequency shifts, and it may be impossible without further information or complementary techniques to separate and quantify these two adsorption processes. SCTFs with more spatially coherent geometry, including at the tips, could be used for future QCM adsorption studies for the purpose of isolating the $\delta\nu_N$ shift caused by the density difference between retained liquid and adsorbate.

6. Conclusion

While the FOA does not take into account the actual geometry of a SCTF (3D nanostructures), the FOA is a simple method to separate by only a QCM measurement between the effects of the areal inertial mass of retained liquid and the bulk properties on isotope exchange of liquids over a surface comprising highly ordered 3D nanostructures. Surface modification by an adsorption process, for example, may modulate the values of C, $\delta\nu_1$, $\delta\Gamma^{H_2O}$, $\delta\Gamma^{H_2O}_{SCTF}$, and γ. The effects of adsorbate particle size, the areal inertial mass of adsorbate that attaches within the SCTF, and SCTF topology (e.g., the spacing between nanostructures of a SCTF) on the quantity of liquid that is retained during QCM measurement of adsorption processes are all of interest for further study.

The results described here have important implications regarding the interpretation of QCM data for adsorption processes into SCTFs. The QCM frequency response for an adsorption process within a SCTF includes a component that is proportional to the density difference between adsorbate and liquid instead of the adsorbate density and hence reduces QCM sensitivity. Comparison of QCM results for adsorption processes into SCTF with optical (GE) results may be very different compared to adsorption processes on flat surfaces. As SCTF surfaces continue to be used for biosensing, tissue scaffolding, and responsive surface applications, the continuing development of QCM data analysis algorithms for use with 3D surfaces may prove immensely useful.

Acknowledgments

The authors acknowledge financial support from The Procter and Gamble Company and the National Science Foundation under award EPS-1004094. The authors thank R.P. Richter for fruitful discussions.

References

[1] F. Höök, M. Rodahl, B. Kasemo, P. Brzezinski, Proc. Natl. Acad. Sci. USA 95 (21) (1998) 12271–12276.
[2] K.B. Rodenhausen, M. Guericke, A. Sarkar, T. Hofmann, N. Ianno, M. Schubert, T.E. Tiwald, M. Solinsky, M. Wagner, Thin Solid Films 519 (2011) 2821–2824.
[3] T. Kasputis, A. Pieper, M. Schubert, A.K. Pannier, Thin Solid Films 571 (2014) 637–643.
[4] T. Nihira, T. Mori, M. Asakura, Y. Okahata, Langmuir 27 (6) (2011) 2107–2111.
[5] K.B. Rodenhausen, B.A. Duensing, T. Kasputis, A.K. Pannier, T. Hofmann, M. Schubert, T.E. Tiwald, M. Solinsky, M. Wagner, Thin Solid Films 519 (2011) 2817–2820.
[6] F. Höök, B. Kasemo, T. Nylander, C. Fant, K. Sott, H. Elwing, Anal. Chem. 73 (24) (2001) 5796–5804.
[7] E. Bittrich, K.B. Rodenhausen, K.-J. Eichhorn, T. Hofmann, M. Schubert, M. Stamm, P. Uhlmann, Biointerphases 5 (159) (2010) 159–167.
[8] J.J.R. Stålgren, J. Eriksson, K. Boschkova, J. Colloid Interf. Sci. 253 (1) (2002) 190–195.
[9] G. Wang, M. Rodahl, M. Edvardsson, S. Svedhem, G. Ohlsson, F. Höök, B. Kasemo, Rev. Sci. Instrum. 79 (7) (2008) 075107.
[10] I. Reviakine, D. Johannsmann, R.P. Richter, Anal. Chem. 83 (2011) 8838–8848.
[11] A. Domack, O. Prucker, J. Rühe, D. Johannsmann, Phys. Rev. E 56 (1) (1997) 680–689.
[12] R.P. Richter, A.R. Brisson, Biophys. J. 88 (5) (2005) 3422–3433.
[13] R.A. May, D.W. Flaherty, C.B. Mullins, K.J. Stevenson, J. Phys. Chem. Lett. 1 (8) (2010) 1264–1268.
[14] L. Macakova, E. Blomberg, P.M. Claesson, Langmuir 23 (24) (2007) 12436–12444.
[15] A. Tiraferri, P. Maroni, D. Caro Rodríguez, M. Borkovec, Langmuir 30 (17) (2014) 4980–4988.
[16] R.J. Green, R.A. Frazier, K.M. Shakesheff, M.C. Davies, C.J. Roberts, S.J. Tendler, Biomaterials 21 (18) (2000) 1823–1835.
[17] P. Gomes, E. Giralt, D. Andreu, J. Immunol. Methods 235 (1–2) (2000) 101–111.
[18] M.J. Swann, L.L. Peel, S. Carrington, N.J. Freeman, Anal. Biochem. 329 (2) (2004) 190–198.
[19] J. Escorihuela, M.A. González-Martínez, J.L. López-Paz, R. Puchades, A. Maquieira, D. Gimenez-Romero, Chem. Rev. 115 (1) (2015) 265–294. pMID: 2545630.
[20] K.B. Rodenhausen, M. Schubert, Thin Solid Films 519 (2011) 2772–2776.
[21] K.B. Rodenhausen, T. Kasputis, A.K. Pannier, J.Y. Gerasimov, R.Y. Lai, M. Solinsky, T.E. Tiwald, A. Sarkar, T. Hofmann, N. Ianno, M. Schubert, Rev. Sci. Instrum. 82 (2011) 103111.
[22] R.P. Richter, K.B. Rodenhausen, N.B. Eisele, M. Schubert, in: K. Hinrichs, K.-J. Eichhorn (Eds.), Ellipsometry of Functional Organic Surfaces and Films, Springer, 2014.
[23] K. Robbie, M.J. Brett, J. Vac. Sci. Technol. A 15 (3) (1997) 1460–1465.
[24] K. Robbie, G. Beydaghyan, T. Brown, C. Dean, J. Adams, C. Buzea, Rev. Sci. Instrum. 75 (4) (2004) 1089–1097.
[25] M.C. Demirel, E. So, T.M. Ritty, S.H. Naidu, A. Lakhtakia, J. Biomed. Mater. Res. B 81B (1) (2007) 219–223.
[26] K.B. Rodenhausen, D. Schmidt, T. Kasputis, A.K. Pannier, E. Schubert, M. Schubert, Opt. Exp. 20 (5) (2012) 5419–5428.
[27] M. Koenig, T. Kasputis, D. Schmidt, K.B. Rodenhausen, K.-J. Eichhorn, A. Pannier, M. Schubert, M. Stamm, P. Uhlmann, Anal. Bioanal. Chem. 406 (28) (2014) 7233–7242.
[28] T. Kasputis, A. Pieper, K.B. Rodenhausen, D. Schmidt, D. Sekora, C. Rice, E. Franke-Schubert, M. Schubert, A.K. Pannier, Acta Biomater. 18 (2015) 88–99.
[29] A. Lakhtakia, R. Messier, Sculptured Thin Films: Nanoengineered Morphology and Optics, SPIE, Bellingham, Washington, 2005.
[30] D. Schmidt, C. Müller, T. Hofmann, O. Inganäs, H. Arwin, E. Schubert, M. Schubert, Thin Solid Films 519 (9) (2011) 2645–2649.
[31] D. Liang, D. Schmidt, H. Wang, E. Schubert, M. Schubert, Appl. Phys. Lett. 103 (11) (2013) 111906.
[32] J.D. Driskell, S. Shanmukh, Y. Liu, S.B. Chaney, X.-J. Tang, Y.-P. Zhao, R.A. Dluhy, J. Phys. Chem. C 112 (4) (2008) 895–901.
[33] S. Martin, G. Frye, K. Wessendorf, Sensor. Actuat. A – Phys. 44 (3) (1994) 209–218.
[34] K. Rechendorff, M.B. Hovgaard, M. Foss, F. Besenbacher, J. Appl. Phys. 101 (11) (2007) 114502.
[35] V.S.J. Craig, M. Plunkett, J. Colloid Interf. Sci. 262 (1) (2003) 126–129.
[36] S.M. Notley, M. Eriksson, L. Wågberg, J. Colloid Interf. Sci. 292 (1) (2005) 29–37.
[37] I.G. Sedeva, R. Fetzer, D. Fornasiero, J. Ralston, D.A. Beattie, J. Colloid Interf. Sci. 345 (2) (2010) 417–426.
[38] J.D. Kittle, X. Du, F. Jiang, C. Qian, T. Heinze, M. Roman, A.R. Esker, Biomacromolecules 12 (8) (2011) 2881–2887.
[39] T. Köhnke, Å. Östlund, H. Brelid, Biomacromolecules 12 (7) (2011) 2633–2641.
[40] D. Schmidt, B. Booso, T. Hofmann, E. Schubert, A. Sarangan, M. Schubert, Appl. Phys. Lett. 94 (1) (2009) 011914.
[41] D. Schmidt, B. Booso, T. Hofmann, E. Schubert, A. Sarangan, M. Schubert, Opt. Lett. 34 (7) (2009) 992–994.
[42] D. Schmidt, A.C. Kjerstad, T. Hofmann, R. Skomski, E. Schubert, M. Schubert, J. Appl. Phys. 105 (11) (2009) 113508.
[43] D. Schmidt, E. Schubert, M. Schubert, Phys. Stat. Sol. (a) 205 (4) (2008) 748–751.
[44] D. Schmidt, E. Schubert, M. Schubert, Appl. Phys. Lett. 100 (1) (2012) 011912.
[45] M. Rodahl, F. Höök, C. Fredriksson, C.A. Keller, A. Krozer, P. Brzezinski, M. Voinova, B. Kasemo, Faraday Discuss. 107 (1997) 229–246.
[46] F. Höök, M. Rodahl, P. Brzezinski, B. Kasemo, Langmuir 14 (4) (1998) 729–734.
[47] P. Bingen, G. Wang, N.F. Steinmetz, M. Rodahl, R.P. Richter, Anal. Chem. 80 (23) (2008) 8880–8890.
[48] G. Sauerbrey, Z. Phys. A-Hadron. Nucl. 155 (2) (1959) 206–222.
[49] T.K. Ghanty, V.N. Staroverov, P.R. Koren, E.R. Davidson, J. Am. Chem. Soc. 122 (6) (2000) 1210–1214.
[50] M.B. Hovgaard, K. Rechendorff, J. Chevallier, M. Foss, F. Besenbacher, J. Phys. Chem. B 112 (28) (2008) 8241–8249.
[51] A. Dolatshahi-Pirouz, T. Jensen, K. Kolind, C. Bünger, M. Kassem, M. Foss, F. Besenbacher, Colloid. Surface. B 84 (1) (2011) 18–25.
[52] A. Borovikov, Instrum. Exp. Tech.-U 19 (1) (1976) 223–224.
[53] K.K. Kanazawa, J.G. Gordon, Anal. Chem. 57 (8) (1985) 1770–1771.
[54] B. Du, I. Goubaidoulline, D. Johannsmann, Langmuir 20 (24) (2004) 10617–10624.
[55] J.C. Munro, C.W. Frank, Macromolecules 37 (3) (2004) 925–938.
[56] E.F. Irwin, J.E. Ho, S.R. Kane, K.E. Healy, Langmuir 21 (12) (2005) 5529–5536.

[57] G.S. Kell, J. Chem. Eng. Data 12 (1) (1967) 66–69.
[58] L. Daikhin, E. Gileadi, G. Katz, V. Tsionsky, M. Urbakh, D. Zagidulin, Anal. Chem. 74 (3) (2002) 554–561.
[59] T. Kasputis, M. Koenig, D. Schmidt, D. Sekora, K.B. Rodenhausen, K.-J. Eichhorn, P. Uhlmann, E. Schubert, A.K. Pannier, M. Schubert, M. Stamm, J. Phys. Chem. C 117 (27) (2013) 13971–13980.
[60] D. Schmidt, M. Schubert, J. Appl. Phys. 114 (8) (2013) 083510.
[61] C. Yaws, The Yaws Handbook of Thermodynamic Properties for Hydrocarbons and Chemicals, Gulf Publishing Company, 2006.
[62] G. Zhang, Macromolecules 37 (17) (2004) 6553–6557.
[63] H.D. Chirra, J.Z. Hilt, Langmuir 26 (13) (2010) 11249–11257.
[64] J.P. Spatz, A. Roescher, M. Möller, Adv. Mater. 8 (4) (1996) 337–340.
[65] R. Glass, M. Arnold, J. Blümmel, A. Küller, M. Möller, J. Spatz, Adv. Funct. Mater. 13 (7) (2003) 569–575.
[66] J.B. Taylor, J.S. Rowlinson, Trans. Faraday Soc. 51 (1955) 1183–1192.
[67] V.A. Sirotkin, I.A. Komissarov, A.V. Khadiullina, J. Phys. Chem. B 116 (2012) 4098–4105.